AGU100 ADVANCING EARTH AND SPACE SCIENCE

JGR

Journal of Geophysical Research: Atmospheres

RESEARCH ARTICLE

10.1029/2017JD027877

Key Points:
- PMF analysis of monthlong hourly major constituents and trace elements in urban Shanghai resolved eight $PM_{2.5}$ source factors
- Benefits of high-time resolution were demonstrated by comparative analysis of PMF solutions with 1-, 4-, and 6-hr averaging data sets
- Source profile mixing and higher rotational ambiguity were observed in PMF solutions of reduced time-resolution data sets

Supporting Information:
- Supporting Information S1
- Data Set S1

Correspondence to:
L. Qiao, L. Li, and J. Z. Yu,
qiaolp@saes.sh.cn;
lili@saes.sh.cn;
jian.yu@ust.hk

Citation:
Wang, Q., Qiao, L., Zhou, M., Zhu, S., Griffith, S., Li, L., & Yu, J. Z. (2018). Source apportionment of $PM_{2.5}$ using hourly measurements of elemental tracers and major constituents in an urban environment: Investigation of time-resolution influence. *Journal of Geophysical Research: Atmospheres*, *123*, 5284–5300. https://doi.org/10.1029/2017JD027877

Received 12 OCT 2017
Accepted 13 APR 2018
Accepted article online 25 APR 2018
Published online 16 MAY 2018

Source Apportionment of $PM_{2.5}$ Using Hourly Measurements of Elemental Tracers and Major Constituents in an Urban Environment: Investigation of Time-Resolution Influence

Qiongqiong Wang[1], Liping Qiao[2], Min Zhou[2], Shuhui Zhu[2], Stephen Griffith[1], Li Li[2], and Jian Zhen Yu[1,3]

[1]Department of Chemistry, Hong Kong University of Science and Technology, Hong Kong, China, [2]State Environmental Protection Key Laboratory of the Formation and Prevention of Urban Air Pollution Complex, Shanghai Academy of Environmental Sciences, Shanghai, China, [3]Division of Environment, Hong Kong University of Science and Technology, Hong Kong, China

Abstract We demonstrate with field data the benefit of using high-time-resolution chemical speciation data in achieving more robust source apportionment of fine particulate matter ($PM_{2.5}$) using positive matrix factorization (PMF). Hourly composition data were collected over a month in Shanghai, including four inorganic ions, 13 elements, organic, and elemental carbon. PMF analysis of the hourly data set (PMF_{1h}) resolves eight factors: secondary nitrate/sulfate, vehicular/industrial emissions, coal combustion, secondary sulfate, tire wear, Cr and Ni point source, residual oil combustion, and dust, with the first three being the major ones and each contributing to >20% of $PM_{2.5}$ mass. To characterize the benefit gained from time resolution, we carried out separate PMF analyses of 4- and 6-hr averaged data of the same data set (PMF_{6h} and PMF_{4h}). PMF_{6h} and PMF_{4h} produce an eight-factor solution sharing similar factors to those by PMF_{1h} but show less stability and more mixing in source profiles. Profile mixing was especially noticeable for tire wear, coal combustion, and Cr and Ni point source in PMF_{6h}, as the 6-hr averaging significantly decreased between-sample variability and increased rotational ambiguity. While the three sets of PMF solutions were similar in contributions for factors with major species as source markers (e.g., secondary nitrate/sulfate), larger variations existed for factors with trace species as markers due to mixing of major species in the profiles and higher rotational uncertainties in PMF_{4h} and PMF_{6h}. Our results indicate that hourly time series of elements and major components could achieve more robust source apportionment through better capturing of diurnal-scale dynamics in source activities.

1. Introduction

Airborne fine particulate matter ($PM_{2.5}$) has garnered considerable global attention due to its impact on climate change, visibility reduction, and human health (Nel, 2005; Ramanathan et al., 2001). Knowledge of emission sources and the contributions is essential to improve air quality. Positive matrix factorization (PMF; Paatero & Tapper, 1994) is a widely used receptor model to apportion source contributions to $PM_{2.5}$ level at a receptor site. Traditional source apportionment studies often rely on filter-based daily or subdaily measurements of elements and compounds. The integrated filter sampling has the advantage of analyzing more species including elements and even trace organic species, which can provide additional aerosol chemical composition and source information (Hu et al., 2010; Wang et al., 2017). However, the daily or subdaily time resolution from these filter-based measurements loses the dynamic information of source activity at the diurnal time scale. In addition, due to the sample size requirement to achieve a robust PMF result, traditional filter-based measurements often spanned one year or more (Qiao et al., 2016) or combined from multiple sites (Huang et al., 2014). The long-time span data posed a potential risk of source profile changing during the study periods (Canonaco et al., 2015), which violates the PMF assumptions.

Online quantification of individual elements or molecules in atmospheric PM with hourly time resolution has been gradually achieved over the past decade (e.g., Phillips-Smith et al., 2017; ten Brink et al., 2007; Williams et al., 2006). Such online instruments for $PM_{2.5}$ components deployed in this work include the following: Monitor for AeRosols and GAses (MARGA for measuring the inorganic aerosol components, including Cl^-, NO_3^-, SO_4^{2-}, NH_4^+, Na^+, K^+, Ca^{2+}, and Mg^{2+}; Griffith et al., 2015; ten Brink et al., 2007), semicontinuous OC/EC analyzer for carbonaceous materials (i.e., organic carbon and elemental carbon, OC and EC; Kim

et al., 2006), and the recently commercially available Xact 625 Particulate Metals Monitor for elements (Phillips-Smith et al., 2017).

The highly time-resolved measurements are intrinsically advantageous for source apportionment analysis, as they are able to capture diurnal scale dynamic processes related to primary source activity (e.g., vehicular emissions) and secondary aerosol formation. Such diurnal variations can be compared with rapid change in meteorological conditions and gas pollutants, thereby serving as supportive evidence in the source identification. In addition, the high-time-resolution data provide the opportunity to do the source apportionment for short periods (e.g., several weeks to months).

The availability and utility of the highly time-resolved trace element data are especially notable for source apportionment, as a number of trace elements are effective indicators for a few common aerosol sources, for example, Ca, Fe, and Mn for dust; Ni and V for residue oil combustion; and As and Se for coal combustion. There are a very small number of source apportionment studies exploring the combined high-resolution data set including trace element measurements (Gao et al., 2016; Peng et al., 2016; Richard et al., 2011; Sofowote et al., 2014). Among them only Peng et al. (2016) paid attention to characterize the benefit gained from time resolution in comparison with source apportionment relying on daily/subdaily time series measurements.

A survey of the literature for past source apportionment studies in China indicates that up to now, source apportionment using online data has been mainly based on the Aerodyne Aerosol Mass Spectrometer (AMS) or Aerosol Chemical Speciation Monitor (ACSM) for PM_1 (Li, Sun, et al., 2017). The AMS or ACSM provide data of ion fragments, which are less uniquely linked to aerosol sources than the molecular or elemental tracers, as the molecular information is partially lost in the process of forming fragment ions in AMS or ACSM. Source apportionment studies based on online aerosol molecular/elemental composition data in China are relatively scarce. Only a few studies are found in the literature, with most of them are conducted in Jing-Jin-Ji region (Gao et al., 2016; Li, Chang, et al., 2017; Li, Ma, et al., 2017; Liu et al., 2017; Peng et al., 2016; Tian et al., 2017), among which only Peng et al. (2016) and Gao et al. (2016) incorporated inorganic ions, OC, EC, and elements. For the Yangtze River Delta (YRD) region, only one study was found (Wang et al., 2016), in which principle component analysis of major inorganic ions alone were used for source apportionment. Studies utilizing the full suite of online measurements, major components plus elements have not been documented for the YRD region yet.

Shanghai is the financial center of the YRD region and has a population of more than 24 million over 6,340 km^2. The city has experienced frequent $PM_{2.5}$ pollution episodes in recent years, with the concentration reaching as high as 200–800 $\mu g/m^3$ (Feng et al., 2012; Li et al., 2014; Wang et al., 2015), far exceeding the National Ambient Air Quality Standards of China (75 $\mu g/m^3$ for 24-hr average, and 35 $\mu g/m^3$ for annual average). In this work, we carried out a PMF analysis of $PM_{2.5}$ sources using hourly data including inorganic ion species, OC, EC, and trace elements, measured in Shanghai during 1–25 December 2014. The aim is to explore with the field data the time-resolution impact on PMF apportionment using the averages of the hourly data, more specifically, to characterize the benefits gained from the enhanced data time resolution in terms of providing improved source apportionment results. This will help to identify the specific advantages of high-resolution data and to understand differences with PMF source apportionment results obtained with daily/subdaily resolution measurements, for which a significantly larger database and understanding have been accumulated. The results from this work will also help to guide efforts balancing data collection frequency and obtaining sufficient materials for high-quality detection by the instruments.

2. Methods

2.1. Sampling and Experiments

All the measurements were conducted at a monitoring site located on the rooftop of a five-story building at the Shanghai Academy of Environmental Science (31.17°N, 121.43°E) in the southwest of the central urban area of Shanghai (Qiao et al., 2014; Wang et al., 2015). The site is mostly surrounded by commercial properties and residential dwellings and could be regarded as a representative urban site influenced by a wide mixture of emission sources. The meteorological parameters, including temperature (T), relative humidity (RH), and

wind speed (WS), were monitored at the same site. Gaseous pollutants, including nitrogen oxides (NO_x), carbon monoxide (CO), and sulfur dioxide (SO_2), were also measured.

The monitoring instruments for $PM_{2.5}$, water-soluble inorganic species, and carbonaceous materials have been described in detail elsewhere (Qiao et al., 2014). Briefly, the concentration of $PM_{2.5}$ was measured by an online beta attenuation particulate monitor (FH 62 C14 series, Thermo Fisher Scientific). Carbonaceous materials (OC and EC) were monitored by a semicontinuous OC/EC analyzer (model RT-4, Sunset Laboratory, Tigard, OR, USA). The water-soluble inorganic species (Cl^-, NO_3^-, SO_4^{2-}, Na^+, NH_4^+, K^+, Mg^{2+}, and Ca^{2+}) were measured by MARGA (Model ADI 2080, Applikon Analytical B.V.).

Concentrations of 22 elements (K, Ca, V, Cr, Mn, Fe, Co, Ni, Cu, Zn, Ga, As, Se, Ag, Cd, Sn, Sb, Ba, Au, Hg, Tl, and Pb) in $PM_{2.5}$ were monitored by an ambient elemental monitor (Xact® 625 Ambient Continuous Multi-metals Monitor, Cooper Environmental Services, Tigard, OR, USA) using nondespersive X-ray fluorescence (XRF) analysis (Battelle, 2012). The hourly sampling duration was chosen to match the sampling frequency of MARGA and RT-ECOC instruments. Ambient air was introduced through a verified $PM_{2.5}$ cyclone inlet and deposited on a Teflon filter tape at the flow rate of 16.7 L/min. The PM deposit was then advanced into the analysis area for XRF analysis at each hour while the next sample was collected. Among the monitored elements, five elements (Co, Sn, Sb, Au, and Tl) were excluded due to over 95% of the data being below detection (i.e., zero concentration); Ag and Cd were also excluded as ~50% and ~80% of the data falling below their respective instrument MDL (Ag: 0.0043 μg/m^3; Cd: 0.0058 μg/m^3; Table S1). Hg and Ga were not included as off-line filter-based data were not available for quality validation. The sampling period starts at 11:00 a.m. 1 December and ends at 19:00 p.m. 25 December 2014. About 70-hr were excluded due to invalid sampling or sampling failure by MARGA or Xact 625 (see Text S1). The valid data rate is 88%.

2.2. Positive Matrix Factorization

The PMF model is a receptor model widely used to resolve pollution sources and quantify the source contributions to ambient concentrations (Paatero & Tapper, 1994). It decomposes the measured data matrix into factor profile and factor contribution matrix, on the basis of finding the minimum value of the Q function, with nonnegative constraints (equations (1) and (2)):

$$x_{ij} = \sum_{k=1}^{p} g_{ik} f_{kj} + e_{ij}, g_{ik} \geq 0, f_{kj} \geq 0 \quad (1)$$

$$Q = \sum_{i=1}^{n} \sum_{j=1}^{m} \left[\frac{e_{ij}}{u_{ij}} \right]^2 \quad (2)$$

x_{ij} is the measured concentration, g_{ik} is the source contribution of the kth factor to the ith sample, and f_{kj} is the factor profile of jth species in the kth factor. e_{ij} is the residual, and u_{ij} is the uncertainty. u_{ij} was calculated as (x_{ij} × error fraction + 1/3 × MDL; Reff et al., 2007), where MDL is the method detection limit. The MDL values are listed in Table S1. They are retrieved from Jeong et al. (2016) and Phillips-Smith et al. (2017) for Xact measured elements, Makkonen et al. (2012) for MARGA ions, and Malaguti et al. (2015) for OC and EC. For data below MDL, the uncertainty was set as 5/6 × MDL (Norris et al., 2014). The error fractions were initialized according to the above references (0.1 for the elements and 0.15 for MARGA ions and 0.15 for OC and EC) and finally scaled to 0.21 for elements and 0.12 for OC and EC, which give better model performance for elements (especially for Cr and Ni which showed larger variation), and balanced scaled residuals from various instruments (Crippa et al., 2013).

In this study, the Environmental Protection Agency (EPA) PMF version 5.0 was used to perform the analysis (Norris et al., 2014), which provides three uncertainty estimation methods to examine the robustness of the solution, namely, bootstrap (BS), displacement (DISP), and bootstrap combined displacement (BS-DISP). BS means randomly resamples the original data matrix and recomputes the model solution. The BS factors are mapped to the base factor with which the correlation of factor contributions is highest, and exceeds a user-selected threshold (default $R \geq 0.6$). The percentage of mapping can provide the reproducibility of different factors. DISP involves displacing each element f_{ij} in the factor profile matrix far from their base value until the change of Q reaches the predefined maximum change (dQ^{max}). In DISP, sometimes the factors change so much that they change identities yielding a factor swap. The extent of the factor swap can indicate the uncertainty of different factors. BS-DISP is a combination of the BS and DISP methods. The elements from

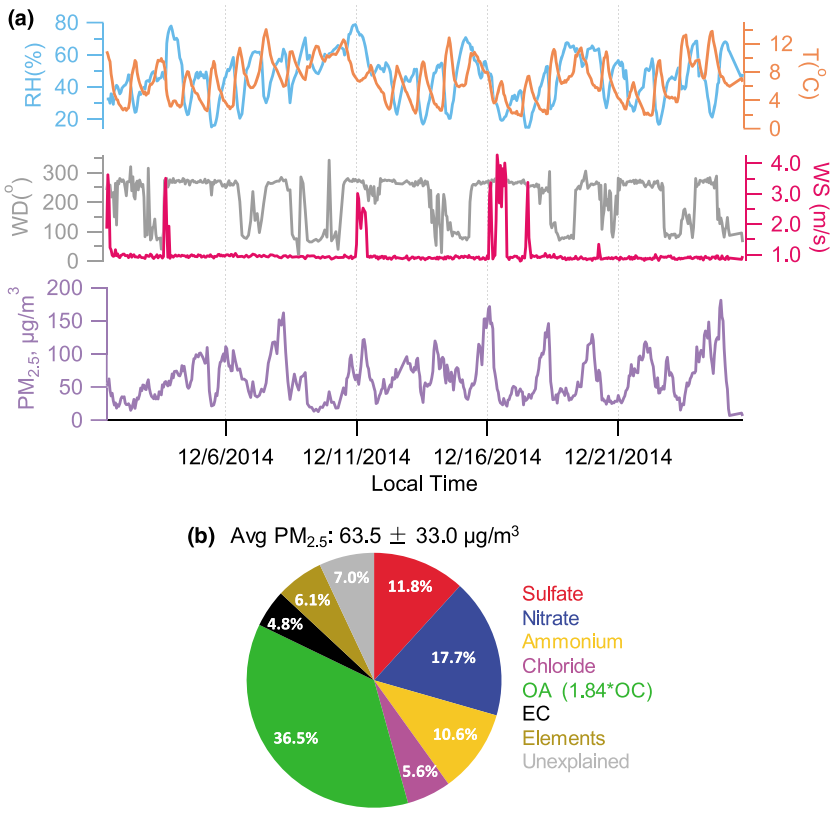

Figure 1. The time series of hourly meteorological parameters (temperature [T], relative humidity [RH], wind speed [WS], and wind direction [WD]) and (a) $PM_{2.5}$ concentrations and (b) average $PM_{2.5}$ chemical composition. (OA = 1.84*OC, Canagaratna et al., 2015).

factor profiles resolved using the resampled data matrix are displaced. BS mainly evaluates random errors of the solution and partially rotational ambiguity, which indicates the possibility of multiple mathematical solutions with the same *Q* value. DISP only evaluates the rotational ambiguity of the solution. BS-DISP evaluates both random errors and rotational ambiguity. The three uncertainty methods can also provide a distribution range of the factor profiles through resampling for multitimes and displacing with the *Q* value change within the preset value. Further details related to the error estimation methods can refer to Brown et al. (2015), Paatero et al. (2014), and Vossler et al. (2016).

3. Results and Discussion

The pollution episodes occurred mostly in winter, due to more frequent stagnant atmospheric conditions and enhanced local and regional emissions (Wang et al., 2015). The monitoring data for this work were collected during 1–25 December 2014. The time series of hourly meteorological parameters and $PM_{2.5}$ concentrations and average $PM_{2.5}$ chemical composition are shown in Figure 1. The average temperature was 6.6°C, and the RH was 45.6%. West wind prevailed during this period, and the WS was only 0.8–1 m/s in 90% of the time. These conditions are very favorable for pollutant accumulations. Average $PM_{2.5}$ concentrations were 63.5 ± 33.0 μg/m^3, with organic aerosol contributing to 37% of the total mass, by applying the average organic aerosol to OC mass convert factor of 1.84 from Canagaratna et al. (2015). Nitrate, sulfate, and ammonium contributed to 18%, 12%, and 11%, respectively. Measured total elements account for 6% of $PM_{2.5}$ mass on average. The concentration statistics of the measured individual component are summarized in Table 1. The mean concentrations are >70 and 17–300 times the respective MDL for the major components and the 13 elements, respectively. A summary of the diurnal variation of the individual species is shown in Figure S1, and the diurnal variation of the meteorological parameters and gaseous pollutants are shown in Figure S2.

Table 1
Statistics of Hourly Concentrations of $PM_{2.5}$ and Measured Components, Criteria Pollutants, and Meteorological Conditions

	Avg	SD	Min	Max
$PM_{2.5}$ and measured components ($\mu g/m^3$)				
$PM_{2.5}$	63.54	32.96	6.26	180.99
Chloride	3.57	2.25	0.36	13.01
Nitrate	11.24	6.83	1.11	47.27
Sulfate	7.47	3.86	1.71	22.87
Ammonium	6.76	4.04	0.80	25.20
OC	12.59	6.21	3.47	35.58
EC	3.04	1.89	0.43	10.95
K	1.21	0.58	0.17	2.89
Ca	0.71	0.68	0.031	5.79
V	0.0060	0.0048	BD[a]	0.032
Cr	0.012	0.012	0.00021	0.13
Mn	0.085	0.042	0.0078	0.30
Fe	1.19	0.82	0.14	7.40
Ni	0.0068	0.0062	0.0010	0.095
Cu	0.029	0.021	0.0024	0.12
Zn	0.42	0.27	0.030	1.86
As	0.018	0.011	0.00048	0.058
Se	0.0075	0.0047	0.00045	0.031
Ba	0.060	0.050	0.0070	0.45
Pb	0.10	0.065	0.010	0.48
Criteria pollutants and meteorological conditions				
O_3 (ppb)	9.63	9.45	1.03	34.61
CO (ppm)	0.86	0.36	0.23	2.45
SO_2 (ppb)	13.30	7.12	1.15	39.60
NO_x (ppb)	73.31	55.30	16.33	427.53
WS (m/s)	1.03	0.50	0.78	4.26
RH (%)	45.63	14.93	14.81	78.72
T (°C)	6.62	2.81	1.82	14.01

[a]Below detection limit.

3.1. Data Validation and Quality Assessment

The array of online instruments, including $PM_{2.5}$ mass monitor, MARGA, RT-ECOC, and online XRF monitor, was operated according to their respective standard procedures for calibration and routine monitoring. The details are described in Text S1.

As part of data validation process, the online measurements were compared with concentrations obtained with off-line laboratory analysis of collocated daily filter samples ($N = 24$). The filter samples were collected from 09:00 a.m. to 09:00 a.m. using a multichannel $PM_{2.5}$ sampler operating at 16.7 L/min. A total of 24 samples were obtained and subjected to determination of mass and analysis of ions, EC, OC, and elements. Briefly, $PM_{2.5}$ mass was obtained gravimetrically by weighing Teflon filters before and after sampling in a RH and temperature controlled environment (50 ± 5%RH, 20 ± 1°C) using a balance with a precision of 1 μg (Mettler Toledo, Model XP-6). The elements were analyzed by an energy-dispersive XRF spectrometer (PANalytical, Epsilon 5), inorganic ions were analyzed using ion chromatography, and OC and EC were analyzed using a DRI thermal/optical ECOC analyzer (Model 2001A), following the IMPROVE-A protocol. The online data ($N = 512$) were averaged to daily resolution according to the filter sampling time interval for comparison with the off-line filter measurements.

Figure S3 shows the linear regression plots of the online measurements against the filter-based measurements, demonstrating good agreement when visually compared with the 1:1 unity line. Table S2 summarizes the slopes, intercepts, and Pearson correlation coefficient (R_p). Excellent correlations ($R_p > 0.96$) were observed between online and off-line measurements of $PM_{2.5}$ mass and major components. The correlations for elements are also very good, with R_p varying from 0.71 for Ca and Ba to 0.95 for Pb (Table S2). Table S3 lists the bias results, which are calculated to be the mean percentage difference of the 24 paired concentrations. With the reasonably tight correlation, the mean bias could be used to indicate the degree of agreement between online and off-line data. The mean bias was less than 20% for $PM_{2.5}$ and the major components, while it was more variable for the elements, from less than 10% for Cu, Fe, K, Mn, Ni, Se, and Zn to ~30% for As, Ca, Cr, V, and Pb. In the verification study conducted by Battelle for the U.S. EPA, online measurements by the Xact 625 were compared with those measured using off-line analysis by inductively coupled plasma mass spectrometry (Battelle, 2012). The mean bias for six of the above elements (Ca, Cu, Mn, Pb, Se, and Zn) was reported, with 75% for Pb and 0.7–31% for the other five elements (after taking the absolute value of the bias). The bias as determined in our work is comparable or better than those reported in the U.S. EPA-commissioned verification study. This more favorable comparison outcome is most likely attributable to the generally higher ambient concentrations of these elements in our study (Table 1).

The bias for Ba was exceptionally high, reaching 139%. The linearly regression plot for Ba indicates a nearly unit slope value (0.967) but a positive intercept value (0.029 $\mu g/m^3$) that is comparable in magnitude to the average Ba concentration in the samples (0.06 $\mu g/m^3$). This may signal that the Xact 625 filter tape background may have contributed significantly to the positive intercept for Ba. This result suggests that analysis of the blank filter tape should be part of the routine daily quality control checks of the online XRF instrument. We note that this positive bias of Ba would not impact source identification, as PMF relies on data variation for resolving source factors.

3.2. PMF Results of Hourly Data (PMF_{1h})

3.2.1. Factor Number Selection

PMF analysis was applied to the combined hourly data covering 13 elements (K, Ca, V, Cr, Mn, Fe, Ni, Cu, Zn, As, Se, Ba, and Pb), 4 inorganic species (Cl^-, NO_3^-, SO_4^{2-}, NH_4^+), OC and EC data, and $PM_{2.5}$ mass

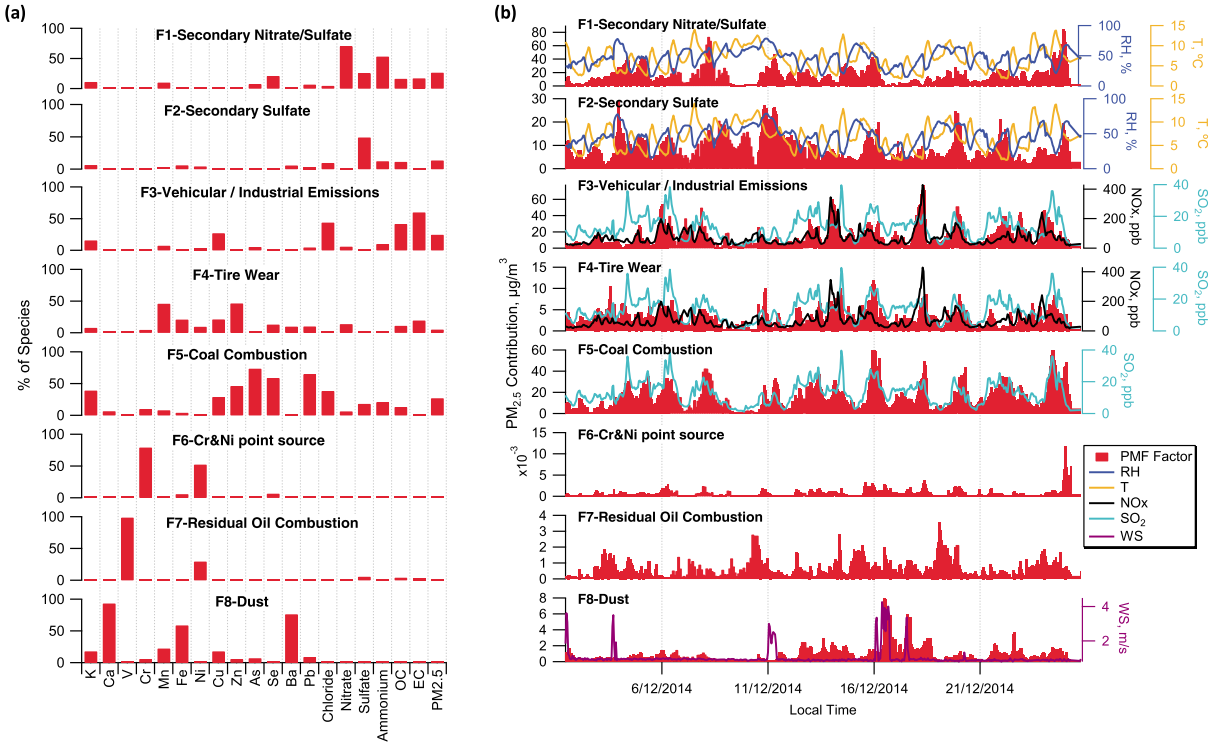

Figure 2. (a) PMF_{1h} resolved factor profiles (percentage of each species in factor) and (b) time series of $PM_{2.5}$ factor contributions by individual factor for the eight-factor solution using hourly data.

concentration. The $PM_{2.5}$ mass concentration was included in PMF as the total variable, which by default was weighted as "weak" (Norris et al., 2014). The 512 × 20 data matrix was subjected to the final PMF analysis.

Four to 17 factors were initially tested to find the optimal factor numbers. The ratio Q/Q_{exp} ($Q_{exp} \approx n \times m - p \times (n + m)$) is shown in Figure S4, where a noticeable decreased value suggests an improved solution, and thus, the parameters experience less dramatic change. We note that the Q/Q_{exp} value trends to 0.4 and this value ideally trends to 1 for a large number of factors. It is possible that the low Q/Q_{exp} value was due to the underestimation of the input errors. While this is not crucial for the validity of the subsequent analysis, future efforts are needed on characterizing measurement uncertainties with the suite of analyzers providing the input data. The Q/Q_{exp} change before eight-factor solution is larger than 14%, while after eight-factor solution, the change is less than 11%). Furthermore, eight factors give the most explainable source profiles. The seven-factor solution cannot separate the Cr&Ni industrial point source from tire wear, while the nine-factor solution produces a residual factor with low loading of all species. The scaled residuals were normally distributed between −4 and 4, and no obvious biases for species from certain instrument were found (Figure S5). The eight-factor solution also shows the most stability, with ≥99% of the BS factors mapped to the base factors, and no factor swaps and no decrease of Q were observed in DISP. Therefore, the eight-factor solution was regarded to be the most plausible outcome. In the BS-DISP uncertainty method, 92% of BS resamples were accepted, and there was a 0.3% decrease of Q and minimal swaps (1–2) for secondary sulfate, secondary nitrate/sulfate, coal combustion, and Cr&Ni point source at the lowest dQ^{max}.

3.2.2. Factor Profile Interpretation

The factor profiles and contributions of the eight-factor solution are shown in Figure 2, and the diurnal variations of individual factor contribution are shown in Figure 3. The correlations between factor contributions and tracer species (i.e., highest loading species in profiles), meteorological parameters, and gas pollutants are shown in Table 2.

The secondary nitrate/sulfate (F1) was identified by high concentrations of nitrate, ammonium, and sulfate (38%). The secondary sulfate factor (F2) is characterized by the high loading of sulfate (47%). The two factors on average contributed to 27% and 13% of total $PM_{2.5}$ mass, respectively (Figure 2). The molar ratio of

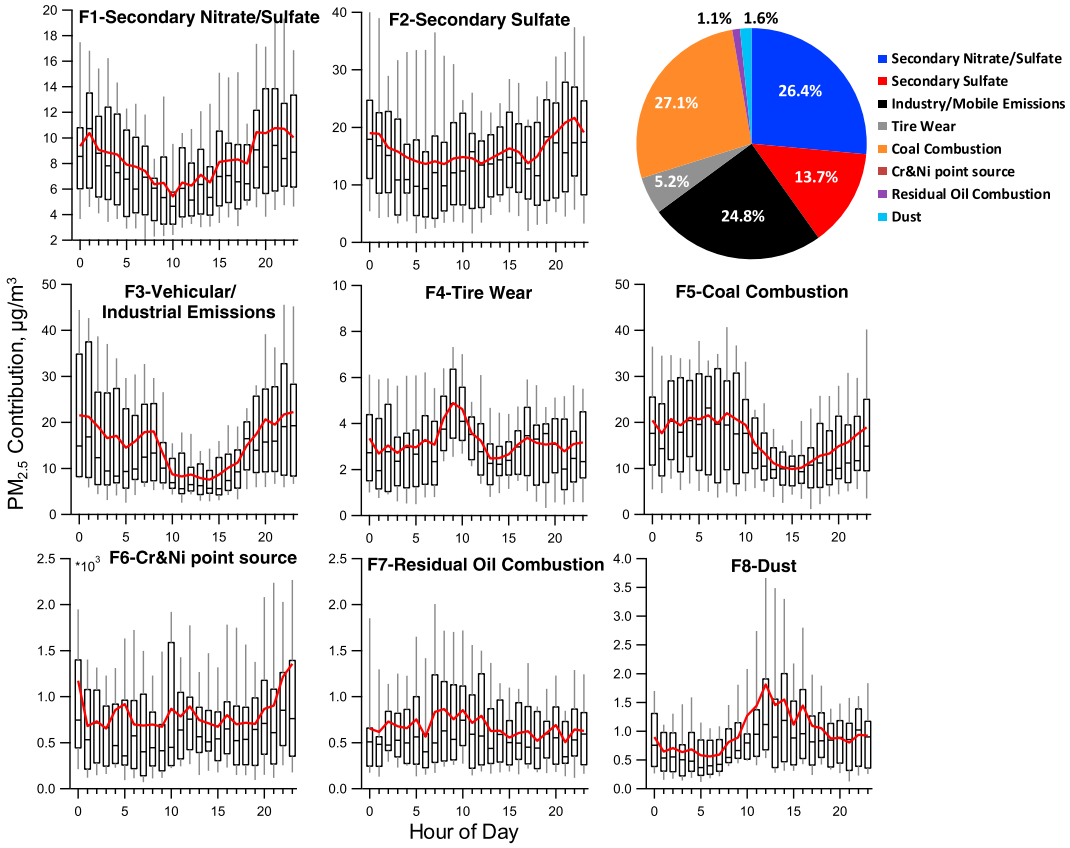

Figure 3. Diurnal variation of individual factor contributions from PMF_{1h} results. (25th and 75th percentile boxes, 10th and 90th percentile whiskers; the dashed line is the median value, and the solid red line is the mean value).

{[NH_4^+]-[NO_3^-]} to [SO_4^{2-}] in F1 is 2.5, suggesting formation of $(NH_4)_2SO_4$, while the molar ratio of [NH_4^+] to [SO_4^{2-}] in F2 is 1.2, suggesting formation of $(NH_4)HSO_4$. The average diurnal variation of F2 showed minor differences between daytime and nighttime values, with two small peaks observed during the day (one around 10:00 a.m. and the other around ~15:00 p.m.; Figure 3), while for F1, much higher contributions were observed at night, suggesting that the two factors were associated with different formation mechanisms. F2 was characterized by the highest correlation with RH (R = 0.50) and CO (R = 0.36), while F1 showed moderate correlations with SO_2 (R = 0.37) and CO (R = 0.35; Table 2). These results suggest that F1 may represent condensation of oxidation products of local emissions in the nighttime plus regional transportation, while in F2, sulfate formation via aqueous phase oxidation and daytime photochemical production may be the dominant pathway. Aqueous phase oxidation of SO_2 is much faster than gas phase processes, especially under humid conditions (Seinfeld & Pandis, 2006). The higher RH in the night facilitates sulfate formation. Sun et al. (2006) also observed increased sulfate formation under high RH in winter in Beijing.

The third factor (F3) has a high abundance of EC, OC, Cu, and Cl^- and is a major $PM_{2.5}$ source, contributing to on average 28% of the total mass. The majority of the OC (48%) and EC (69%) was apportioned to this factor (Figure 2). Vehicle exhaust from tail pipe is an important source for carbonaceous species, and the presence of Cu may originate from both fuel/lubricant combustion and brake abrasions (Adachi & Tainosho, 2004; Pant & Harrison, 2013). The morning rush hour peak at around 8:00 a.m. in the diurnal variation supports the impact of vehicle emissions on this factor (Figure 3). High correlations with NO_x (R = 0.84) and CO (R = 0.77) suggest a strong influence of vehicular/industrial emissions on the factor (Table 1). Huang et al. (2011) reported the emission inventory of NO_x in YRD in 2007 and found that 86% of the NO_x was from industrial sources and 12% from vehicles. The presence of Cl^- in this factor may come from coal burning used in the industrial activities (Huggins & Huffman, 1995; Sun et al., 2013). Thus, this factor is identified as

Table 2
Pearson Correlation (R) of PMF_{1h} Factor Contributions With Corresponding Tracer Species, Meteorological Parameters (Temperature [T], Relative Humidity [RH], and Wind Speed [WS]), and Gas Concentrations (SO_2, NO_x, and CO)

PMF factor	Tracer species[a]		T	RH	WS	SO_2	NO_x	CO
Secondary nitrate/sulfate	NO_3^-	0.968	0.20	0.22	−0.03	**0.37**	−0.05	**0.35**
Secondary sulfate	SO_4^{2-}	0.685	−0.08	**0.50**	0.09	0.02	0.07	**0.36**
Vehicular/industrial emissions	EC	0.930	−0.22	0.17	−0.13	0.39	**0.84**	**0.77**
Tire wear	Mn	0.754	0.01	0.00	−0.07	**0.50**	**0.47**	**0.49**
Coal combustion	As	0.948	−0.22	0.00	−0.02	**0.71**	0.33	**0.53**
Cr&Ni point source	Cr	0.966	−0.02	0.02	0.07	0.31	0.22	**0.35**
Residual oil combustion	V	0.997	**0.30**	0.27	0.05	−0.13	0.18	0.05
Dust	Ca	0.989	−0.05	**−0.54**	**0.44**	0.21	0.07	−0.11

Note. The highest correlation coefficients for each factor are denoted in bold.
[a]Tracer species indicate the species with highest loading in the factor profiles.

vehicular/industrial emissions. The higher nighttime than daytime contribution of this factor may suggest influence from the planetary boundary layer height variation. In the daytime, higher boundary height leads to more vertical mixing of the pollutants and facilitates dispersion, while the stagnant nighttime atmosphere easily accumulates pollutants (Liu & Liang, 2010). We note some presence of K in this factor. Considering the copresence of EC, Cl^-, and K, one could not rule out the possibility of the mixing of biomass burning in this factor. Previous studies in this region have resolved a biomass burning factor, either relying on more indicative source tracers (i.e., levoglucosan and mannosan; Feng et al., 2013; Qiao et al., 2016) or seasonal variation provided through yearlong sampling (Du et al., 2017; Zhao et al., 2015). The inherent ambiguity in using K alone to identify biomass burning highlights the need for developing online measurement capabilities for more source specific organic tracers to improve source apportionment accuracy.

Similar to F3, the tire wear factor (F4) is characterized by a sharp morning rush hour peak, but also shows a small broad afternoon rush hour peak, which is not evident in F3. A significantly higher nighttime level (attributed to boundary layer height) is absent in F4 (Figure 2). Moderate correlations with NO_x (R = 0.47), CO (R = 0.49), and SO_2 (R = 0.50) were observed (Table 2). The separation of F4 with F3 was probably attributed to their different source profile characteristics. The factor profile of F4 shows high loading of Zn, Mn, Fe, and Cu (Figure 2), which are often reported to be associated with nonexhaust vehicle emissions such as tire wear (Pant & Harrison, 2013), while the factor profile of F3 are mainly carbonaceous species, which are characteristics of the exhaust emission. However, previous PMF studies in this region based on off-line composition measurements of filter samples did not resolve such a factor (Du et al., 2017; Huang et al., 2014; Qiao et al., 2016), suggesting the benefit of the online high-resolution measurement. The Fe/Ca and Mn/Ca mass ratios in this factor were 44.5 and 6.7, much higher than the natural soil and paved road dust samples (0.8–2.6, 0.01–0.08; Ho et al., 2003), supporting the anthropogenic feature of this factor. The factor contribution to total $PM_{2.5}$ mass was minor, only 6%.

As another major source, the coal combustion factor (F5) contains high loading of metals such as As, Se, Pb, and Cl^- and contributes to 23% of $PM_{2.5}$ mass on average (Figure 2). As and Se are mostly associated with coal combustion emissions (Chen et al., 2013; Vejahati et al., 2010). Good correlations of this factor with SO_2 (R = 0.71) and CO (R = 0.53; Table 2) further support the identification of this factor. Diurnal variation of the factor showed low contribution during the day (Figure 3), which may be due to boundary layer height variation, and indicating the regional characteristic of this factor.

The sixth factor (F6) is characterized by high concentrations of Cr and Ni (Figure 2), which are often used in industrial processes such as plating, tanning, and metallurgy (Borai et al., 2002; Karar et al., 2006). This factor shows best correlation with CO (R = 0.35; Table 2). No diurnal variation was observed (Figure 3), and the time series of this factor showed intense contributions on the last two days of the sampling period (i.e., 24–25 December 2014; Figure 2). The factor still stood out when performing PMF runs without the intense contribution period, indicating the persistence of the source throughout the sampling period. The residual oil combustion factor (F7) was identified by V and Ni (Figure 2), of which V is often used as a tracer for residual oil combustion. The V/Ni ratio in this factor was 3.1, very close to the average value (3.6) in international heavy fuel oils used in the Port of Shanghai (Zhao et al., 2013), suggesting a strong impact of shipping

transportation activities on this factor. No diurnal variation was observed (Figure 3), and the factor only slightly correlated with T (R = 0.30; Table 2). The dust factor (F8) was distinguished by crustal elements Ca, Fe, and Ba (Figure 2). The Fe/Ca and Mn/Ca mass ratios in this factor were 1.1 and 0.03, in agreement with the abundance in soil and paved road dust samples (0.8–2.6, 0.01–0.08; Ho et al., 2003). The factor's diurnal variation showed a broad peak during the daytime (Figure 3), moderate correlation with WS (R = 0.44), and negative correlation with RH (R = −0.54; Table 2), suggesting an influence from meteorological conditions. The three factors, F6–F8, were minor contributors to $PM_{2.5}$, accounting for only 2%, 0.2%, and 1%, respectively.

A sea-salt factor was not resolved despite the coastal location of our study site. This most likely was a result of a lack of Na^+ concentrations in the data matrix for the PMF analysis. Na^+ data were not obtained from MARGA due to its general low level. In future monitoring efforts, it is worth exploring whether prolonging sampling time could improve its detection to enable its use in PMF analysis. Compared with previous source apportionment studies based on off-line measurements of filter samples, this study produced results generally consistent with the winter PMF results in Du et al. (2017), more specifically, the major source contributors of secondary inorganic formation being 40% versus 23% and vehicular emissions being 30% versus 30%. The coal combustion source in this study (27%) probably corresponds to the industry activities and combustion source identified in Du et al. (2017) (28% in total). In comparison with the studies by Huang et al. (2014) and Qiao et al. (2016), this study found lower secondary contribution and much higher coal combustion contribution and vehicular emission. We note that the latter two did not resolve any industry-related sources in their studies. Cross-comparing source apportionment results by different methods are needed in the future to identify deficiencies in various source apportion approaches.

3.2.3. Back Trajectory Analysis of PMF_{1h}-Resolved Sources

Previous studies using source-oriented model indicated the importance of both regional transport and local emissions for the haze episodes in Shanghai. Wang et al. (2014) identified two types of haze episodes in November 2010: when under rather weak wind (WS $<$ 0.5 m/s), local emissions dominant, while under moderate wind (~2 m/s), regional transport from upwind areas contributed most. Li et al. (2015) found that the local emission in Shanghai (~50%) is the largest contributor to the pollution in January 2013, with a similar meteorological condition in this study.

To investigate the influence of air mass origin on different PMF factor contributions, backward trajectory analysis was performed using the Hybrid Single-Particle Lagrangian Integrated Trajectory (HYSPLIT) model (http://www.arl.noaa.gov/ready/hysplit4.html). The 36-hr duration backward trajectories arriving at an altitude of 100 m above ground level over the site were calculated every hour from 1 to 25 December 2014 utilizing the Global Data Assimilation System 1° global meteorological data. The trajectories were then clustered according to the similarity in spatial distribution. An optimum solution of five clusters was extracted according to the change in total spatial variance, and the cluster means are shown in Figure 4. The individual trajectory in each cluster is shown in Figure S6, together with the corresponding average PM compositions. The distribution of meteorological parameters and gas pollutants in each cluster is shown in Figure S7. Clusters 1, 2, and 3 represent continental air masses from the northwest with different trajectory lengths (cluster 1 $>$ 2 $>$ 3), indicating gradually slower air mass. Cluster 1 represents long-range transport air masses from Mongolia (Inner Mongolia) region, while cluster 3 represents air masses from the China Central Plain. Cluster 4 represents flows that recirculate from the surrounding regions in the YRD in all directions covering continental and oceanic areas, resulting in more impact from air masses of local emissions. These four clusters express the dominant trajectories, accounting for 11%, 22%, 45%, and 15% of the total trajectories, respectively. Cluster 5 represents northeast oceanic air masses and contributes 11% to the total trajectories. The increasing trend of PM mass from clusters 1 to 3 was probably due to the accumulation of local emissions under calm meteorological conditions (Figure S7). The highest PM concentrations in cluster 3 indicate the regional transport from the heavily polluted China Central Plain, while the high PM mass in cluster 4 suggests heavy local pollutions. The similarity of PM composition under each cluster indicates the severe background pollution under the weak background winds. Chloride in winter was reported to be mainly associated with coal combustion in a number of studies (e.g., Sun et al., 2013; Ye et al., 2003). In this data set, chloride showed obvious anthropogenic features, for example, high correlation with EC (R = 0.82). The anthropogenic source likely dominated over the sea-salt input, explaining lack of observation of chloride increase in cluster 5.

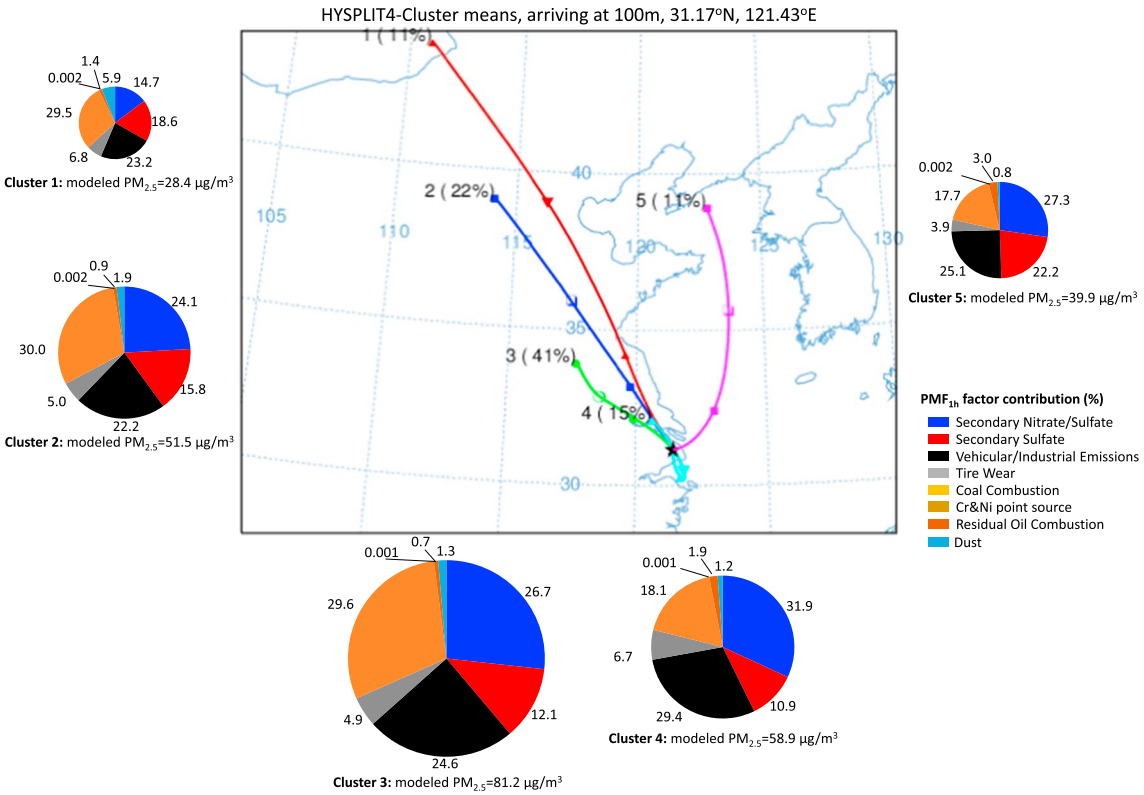

Figure 4. PMF_{1h} factor contribution in different clusters between 1 and 25 December 2014. The center map shows the back trajectory cluster means (indicated by the colored lines). The pie chart components indicate the percentage contribution of individual PMF_{1h} factor (indicated by the surrounding numbers), and the size of the pie chart is proportional to the modeled $PM_{2.5}$ mass in each cluster.

Source contributions of the resolved factors varied with air mass origins, as seen from the comparison of PMF factor contributions in each cluster shown in Figures 4 and S8. Secondary nitrate/sulfate, secondary sulfate, vehicular/industrial emissions, and coal combustion are responsible to the PM pollution in all clusters. The secondary nitrate/sulfate factor showed highest contributions in clusters 3 and 4, with average contributions (21.7 and 18.8 μg/m^3, 27% and 32%) more than 2 times higher than in clusters 1 (4.16 μg/m^3, 15%). Secondary sulfate factor was less affected by the origin of arriving air masses (5.27–9.83 μg/m^3, 11–22%), suggesting contribution from the more localized background air. The slightly higher fractional contribution under cluster 5 (22%) could be due to the higher RH (Figure S7). Vehicular/industrial emissions showed similar trend with secondary nitrate/sulfate factor, with higher mass contributions from trajectories in clusters 3 and 4 than clusters 1, 2, and 5, suggesting both local and regional impact. Coal combustion showed much higher mass contributions under clusters 2 and 3 (15.5 and 24.1), similar to the variation of SO_2 (Figure S7), indicating the strong impact of the regional transport from northern China. Tire wear showed similar contributions under different clusters (1.56–4.01 μg/m^3, 4–7%), supporting influence from local emission sources. Cr&Ni point source showed similar contributions under different air masses, although the high episodes occur under oceanic cluster 5. Residual oil combustion showed higher contributions under oceanic trajectories (clusters 4 and 5), supporting air masses associated with ship emissions. Likewise, dust showed higher contributions under long-range transport trajectories (cluster 1), indicating a superregional input.

3.3. Time-Resolution Impact on PMF

To examine the impact of time resolution on PMF results, two additional data sets were generated by averaging the 1-hr resolution data ($N = 512$) into 4-hr ($N = 145$) and 6-hr ($N = 97$) time intervals. Longer time intervals (e.g., 8 or 12 hr) yielded data sets too small (70 × 20 or 50 × 20) to generate sufficiently robust PMF results. The shorter periods (e.g., 2 or 3 hr) resulted in little difference compared with the hourly data, implying that time series of 2- or 3-hr measurements would also be adequate to capture the source dynamics at this site in the winter. Similar analysis of time-resolution impact would be beneficial for months of lower pollution, for

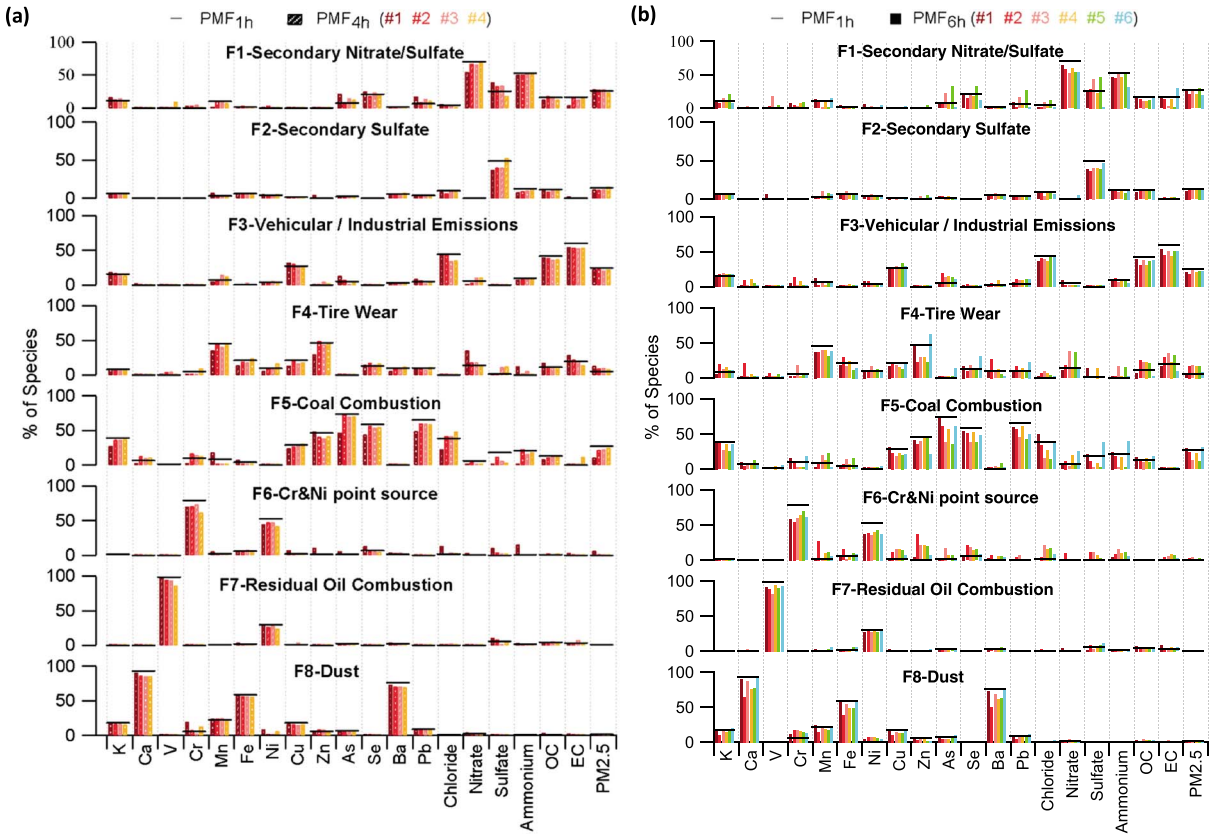

Figure 5. Factor profiles resolved in individual cases of (a) PMF_{4h} and (b) PMF_{6h}. The factor profiles in PMF_{1h} are shown in dashed line.

which ambient concentrations under hourly sampling conditions might approach or fall below the detection limits of some online instruments.

For the 4-hr averaging case, theoretically, there are four different combinations, that is, starting hour from 00:00 (Case #1), 01:00 (Case #2), 02:00 (Case #3), to 03:00 (Case #4) by every hour increase. Take Case #1 as example, the individual sample periods within 24 hr are 00:00–04:00, 04:00–08:00, 08:00–12:00, 12:00–16:00, 16:00–20:00, and 20:00–00:00. Similarly, for the 6-hr average case, there exist six different combinations, that is, starting hour from 00:00 (Case #1) to 05:00 (Case #6) by every hour increase. After averaging, four different data matrices of 145 × 20 from 4-hr average data and six different data matrices of 97 × 20 from 6-hr average data were obtained and subjected to PMF analysis (PMF_{4h} and PMF_{6h}). The previous studies examining time-resolution impact (Peng et al., 2016) did not consider the different averaging combination, which from the results in this study, cannot fully characterize the variations due to coarse time impact. The uncertainty for each averaged data point was calculated according to the error propagation method described earlier.

3.3.1. Factor Profile Variations

In order to compare with PMF_{1h}, a same factor number, that is, eight-factor solution, was chosen for PMF_{4h} and PMF_{6h} data sets. However, it should be noted that for the coarse-time smaller data set, less factors will probably be resolved to keep more robust solution, if no previous 1-h data were available. The eight-factor solutions from the PMF_{4h} and PMF_{6h} data sets were compared with that of PMF_{1h}. The factor profiles of the eight-factor solutions in different cases of PMF_{6h} and PMF_{4h} are shown in Figure 5. Generally, the identified eight factors were similar to those of PMF_{1h}, especially for PMF_{4h}. However, noticeable variations were observed among different cases of PMF_{4h} and PMF_{6h} solutions, mainly for non-source-specific species. As indicated by the coefficient of variation (CV, standard deviation divided by mean), the loadings of source-specific markers in their respective factors from different cases were very stable. In PMF_{4h}, the CV values of the source-specific markers ranged from 3% for dust to 19% for tire wear and coal combustion; in PMF_{6h},

Table 3
Summary of Error Estimation Diagnostics for PMF_{4h} and PMF_{6h} Results

		BS		DISP	BS-DISP		
Case	Q/Q_{exp}	BS factor mapping to base factors <100%	Decrease in Q	Factors swaps at lowest dQ^{max}	#Rejected BS resamples	Decrease in Q	Factors swaps at lowest dQ^{max}
PMF_{4h}							
#1	2.03	Sulfate: 79% Tire wear: 83%	0.009	No swaps	62 out of 100, mainly due to swapping of factors	4.115	All factors swap 2–10 times except residual oil combustion.
#2	2.07	Tire wear:70% Sulfate: 87% Cr&Ni: 92%	0.065	No swaps	75 out of 100, mainly due to swapping of factors	5.335	All factors swap 1–17 times except dust.
#3	2.07	Tire wear: 79% Sulfate: 87% Cr&Ni: 98% Coal: 99%	0.028	No swaps	81 out of 100, mainly due to swapping of factors	7.276	All factors swap 1–13 times except dust.
#4	2.02	Tire wear: 79% Cr&Ni: 84% Sulfate:94% Nitrate:99%	0.027	No swaps	68 out of 100, mainly due to swapping of factors	0.885	All factors swap 2–10 times except dust.
PMF_{6h}							
#1	2.65	Cr&Ni: 98% Sulfate: 94% Tire wear: 96%	1.89	Vehicular/industrial factor and tire wear swap 7 times	Failed[a]		
#2	2.71	Tire wear: 76% Sulfate: 87% Cr&Ni: 94%	1.49	Tire wear: 8 times; nitrate factor: 6 times; vehicular/industrial and sulfate swap once	Failed		
#3	2.69	Tire wear: 89% Cr&Ni: 96% Sulfate: 99%	0.03	No swaps	86 out of 100, mainly due to swapping of factors	1.22	All factors swap 1–18 times.
#4	2.63	Tire wear: 79% Sulfate: 98% Coal, nitrate, Cr&Ni: 99%	0.51	Tire wear and sulfate factor swap once	Failed		
#5	2.62	Tire wear: 93% Sulfate:96%	0.03	No swaps	62 out of 100, due to swapping of factors	2.68	All factors swap 1–4 times.
#6	2.63	Coal: 84% Sulfate: 94% Tire wear: 99%	2.57	Nitrate factor: 3 times Coal: 2 times Tire wear: 4 times	Failed		

[a]Failed due to not enough accepted BS-DISP runs.

the CV ranged from 7% for Cr&Ni point source and residual oil combustion factors to 26% for coal combustion and 49% for tire wear factor in PMF_{6h}. In comparison, the case-to-case variations of non-source-specific species were noticeable, and larger in PMF_{6h} than in PMF_{4h}. For example, the CV of non-source-specific species in the secondary nitrate factor ranged from 14% for K and Se to 200% for Cu in PM_{4h} and 24% for OC to 237% for Zn in PM_{6h}.

In reference to PMF_{1h} solutions, factors in some cases of PMF_{4h} and PMF_{6h} gave more mixed profiles, with slightly lower loading of markers and higher loading of the non-source-specific species. In PMF_{4h}, individual factors showed very similar factor profiles to those in PMF_{1h}, except for Case #1, which showed more profile mixing among tire wear, coal combustion, and Cr&Ni point source (Figure 5a). In PMF_{6h}, secondary sulfate, vehicular/industrial emissions, and residual oil combustion were consistent among different cases and very similar to those in PMF_{1h}; however, secondary nitrate/sulfate, tire wear, coal combustion, Cr&Ni point source, and dust factor showed larger variations among PMF_{6h} cases and noticeable deviations from those in PMF_{1h} were observed in some PMF_{6h} cases (Figure 5b). For example, the PMF_{6h} source profile of the secondary nitrate/sulfate factor in Cases #1, #2, and #4 closely resembled the corresponding PMF_{1h} profile, but Cases #3 and #5 showed more mixed profiles with coal combustion and secondary sulfate associated species (i.e., As, Se, and Pb with SO_4^{2-}), and Case #6 showed more mixed profiles with industry/mobile emission associated species (i.e., OC and EC).

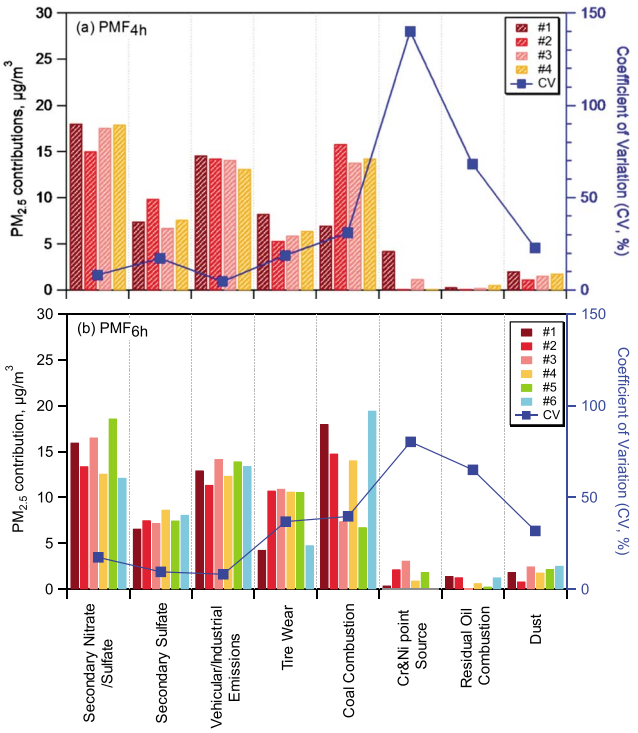

Figure 6. Comparison of average source contributions ($\mu g/m^3$) of individual factors among different cases of (a) PMF_{4h} and (b) PMF_{6h}. The blue squares are coefficient of variation (CV) values of individual factor source contributions across all cases of PMF_{4h} or PMF_{6h}.

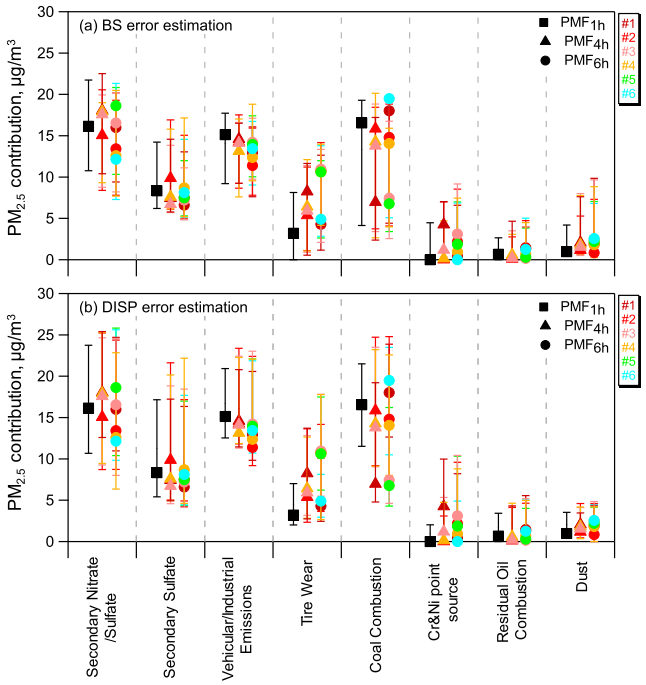

Figure 7. Site comparison of source contribution to $PM_{2.5}$ by individual factor from PMF_{4h} and PMF_{6h} with PMF_{1h}; the whiskers indicate the lower and upper interval estimate from (a) BS and (b) DISP error estimation methods.

More examples of mixed profiles could be identified in PMF_{6h} solutions. Tire wear from Cases #1 and #6 mixed with coal combustion related species (As, Se, and Pb), and Case #2 with dust-related elements (Ca, Fe, and Ba), and Cases #3 and #5 with secondary nitrate/sulfate species (NO_3^- and NH_4^+). Coal combustion in Cases #3 and #5 showed an overall lower loading of markers and Case #6 more mixed with SO_4^{2-} and NH_4^+. Cr&Ni point source from Cases #2, #3, #4, and #5 showed more mixed profiles for the non-source-specific species. Dust from Cases #2, #3, and #4 showed slightly lower loading of the marker species due to mixing to other factors.

The summary of the error estimation diagnostics for each PMF_{4h} temporal case are shown in Table 3. The Q/Q_{exp} values were similar among the different PMF_{4h} cases, varying from 2.02 to 2.07. Most BS factor mappings were larger than 90%, except for tire wear and secondary sulfate and in one case, Cr&Ni point source. Cases #1 and #2 of the PMF_{4h} results showed the most stable DISP and BS-DISP results, with less drop in Q values. Most of the BS resamples were rejected in BS-DISP mainly due to factor swaps, indicating more rotational ambiguity in PMF_{4h} compared with PMF_{1h}.

Table 3 shows the error estimation diagnostics for PMF_{6h} results. The Q/Q_{exp} values ranged from 2.62 to 2.71. Generally, a larger variation in stability for PMF_{6h} was observed, especially for DISP and BS-DISP results. For BS results, while most BS factor mappings were larger than 90%, the mapping of three factors occasionally fell below 90%, with tire wear in three cases, secondary sulfate in one case, and coal combustion in one case, suggesting less reproducibility of these factors. Cases #3 and #5 showed the most stable DISP results with minimum drop of Q and no factor swaps. Cases #1, #2, and #6 of PMF_{6h} involved factor swaps several times especially for tire wear, secondary nitrate, and vehicular/industrial emissions factors. In four out of the six PMF_{6h} cases, the BS-DISP runs failed, due to the insufficient accepted runs, indicating more rotational ambiguity in PMF_{6h} compared with PMF_{4h}.

3.3.2. $PM_{2.5}$ Contribution Variations

The average $PM_{2.5}$ contributions from each factor from different cases in PMF_{4h} and PMF_{6h} are shown in Figure 6, and the time series of $PM_{2.5}$ contributions are shown in Figure S9. Of the eight source factors, secondary nitrate/sulfate, secondary sulfate, and vehicular/industrial emissions showed relatively stable contributions among different cases, with a CV of 5–17% in PMF_{6h} and PMF_{4h}, where the variation can be attributed to the stability of their marker species, all of which are major components of $PM_{2.5}$. For the factors with trace elements as marker species, variation of the non-source-specific species had a notable influence on the average $PM_{2.5}$ contributions. Tire wear showed similar variability in source contributions in the PMF_{4h} solutions (CV: 19%), but larger variations in PMF_{6h} solutions (CV: 40%), with Cases #2, #3, #4, and #5 showing much higher contributions than the other cases, due to factor mixing of the common major species. Coal combustion showed large variations in both PMF_{4h} and PMF_{6h} solutions, with a CV of 31% and 39%, respectively. For the three minor sources, Cr&Ni point source showed the largest CVs (81–141%) due to factor mixing, while residual oil combustion and dust showed relatively lower variations (CV: 23–69%) due to less mixing.

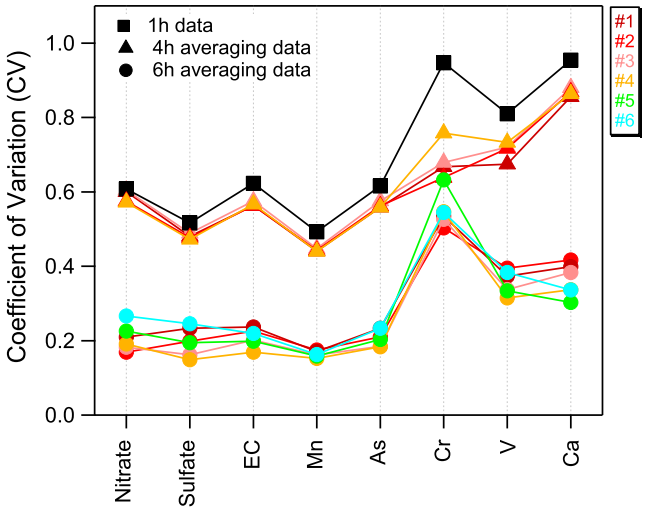

Figure 8. Coefficient of variation (CV) of the tracer species (i.e., highest loading species in factor profiles) for individual factor across different cases for PMF_{1h}, PMF_{4h} and PMF_{6h}.

The variations in source contribution to $PM_{2.5}$ were not only impacted by the mixing of factor profiles, but also the uncertainty in the PMF solutions. Comparison of the average source contributions from individual factors by PMF_{1h}, PMF_{4h}, and PMF_{6h} are displayed in Figure 7, with BS and DISP error estimation ranges also shown (The error estimation ranges for individual cases in PMF_{4h} and PMF_{6h} are shown in Figures S10 and S11). The BS approach mainly evaluates random errors of the solution, which are related to the size of the input data matrix, while DISP only evaluates the rotational ambiguity of the solution (Paatero et al., 2014). For factors with major species as identifying markers, that is, secondary nitrate/sulfate, secondary sulfate, and vehicular/industrial emissions, the average contributions were comparable among PMF_{1h}, PMF_{4h}, and PMF_{6h} solutions. For factors with the trace species as markers, coal combustion showed a large variation, due to the higher/lower mixing of major species in profiles. Tire wear and Cr&Ni point source showed higher contributions due to mixing. While for residual oil combustion and dust, similar contributions were obtained, consistent with the stability of the factor profiles. In terms of the uncertainty ranges, PMF_{4h} and PMF_{6h} showed similar BS uncertainty ranges compared with PMF_{1h}, indicating less impact deriving from the data point reduction in PMF_{4h} and PMF_{6h}, while obvious increased uncertainty ranges by the DISP method in PMF_{4h} and PMF_{6h} were found, indicating larger rotational uncertainty in PMF_{4h} and PMF_{6h} results.

As the average time increased from 4 to 6 hr, the PMF-resolved source contributions showed larger variations. For individual cases, it was observed that those with higher stability (Cases #3 and #5 of PMF_{6h} and Case #1 of PMF_{4h}) showed the largest difference in contribution (i.e., more mixed factor profiles), while the rest exhibiting more rotational ambiguity gave closer contributions to PMF_{1h}.

3.3.3. Insights Into Integrated-Sampling

Data averaging reduces the between-sample variability in the input data, as indicated by the CV of the input tracer species for each factor in PMF_{1h}, PMF_{4h}, and PMF_{6h} (Figure 8). The 6-hr averaging significantly decreases the data variability. For example, the CV of Ca (dust tracer) decreases from 95% for hourly data to 86–88% for 4-hr averaged data, and further down to 30–42% for 6-hr average data. Less variability of the input data generates less distinctive (i.e., more mixed) PMF profiles with increased rotational ambiguity, especially for longer integrated samples. The variability in the results among different cases, especially for PMF_{6h}, was likely caused by differences in the input data and increased rotational ambiguity. The various averages impact interspecies correlations, especially for species with very different variability patterns. The longer the averaging time, the larger the case-to-case difference. The largest difference across cases was 3-hr shifting in PMF_{4h} versus 5-hr shifting in PMF_{6h}. Thus, for sampling of longer integrated time periods, larger variability is associated with the selection of sampling start/end times. Additionally, larger rotational ambiguity caused by less-data-difference also increases the uncertainty of PMF results.

In order to maintain the resolved source information for the lower-time-resolution data, samples collected under different meteorological conditions (e.g., samples collected in different seasons) are needed, or more specific tracer species are needed to compensate the loss of variability due to the longer sampling period. High-time-resolution sampling is needed for a short campaign (e.g., one to two months) with similar meteorological conditions, in order to achieve more robust and rotationally unique solutions.

4. Conclusions

PMF analysis was applied to an hourly data set (PMF_{1h}) covering major components and trace elements in $PM_{2.5}$ collected in Shanghai during 1–25 December 2014. The hourly trace element measurements were crucial in source apportionment as some elements (e.g., As, V, and Ca) are unique source tracers. Eight source factors were resolved using the hourly data set of 520 samples and 19 chemical components. Among them, secondary nitrate/sulfate, vehicular/industrial emissions, and coal combustion were major sources, accounting for 27%, 28%, and 23%, respectively. Trajectory analysis indicated significant impact of local emissions on

most pollution sources, while more regional impact of dust emissions and coal combustion. Thus, control emissions in the upwind areas, especially central plain, as well as control local emissions (mainly vehicles and industries) are both important for the effective pollution control in Shanghai in winter.

Taking advantage of the large data set, we examined the time-resolution impact on PMF solutions through carrying out separate PMF analyses of 4-hr average data (PMF_{4h}) and 6-hr average data (PMF_{6h}). While similar factors were identified, more mixed profiles were resolved by PMF using the lower-time-resolution data, especially in PMF_{6h}. The profile mixing was particularly noticeable for source factors with trace species as identifying markers (i.e., tire wear, coal combustion, and Cr& Ni point source), due to the combined effect of mixed profiles and increased rotational ambiguity in the PMF results of the reduced time-resolution data sets. Such outcomes are likely borne from the reduced sample-to-sample variability in the averaged data matrix. These results support performing PMF analysis with higher-time-resolution measurements and greater variability in the data matrix to achieve more robust source apportionment results.

On the other hand, PMF analyses of 2- and 3-hr averaging periods resulted in little difference compared with the hourly data, implying that time series of 2- or 3-hr measurements would also be adequate for source apportionment at this site in winter. This finding suggests that relying on sampling periods longer than hourly could be considered on days of lower pollution, as ambient concentrations of some species might approach or fall below the detection limits of hourly sampling.

Acknowledgments
This work was supported by the National Environmental Public Welfare Research Program of Ministry of Environmental Protection of China (201409008), Ministry of Science and Technology of China (2014BAC22B03), and National Natural Science Foundation of China (21507088 and 91543130). Chemical composition data are provided as a .csv file in the supporting information section.

References

Adachi, K., & Tainosho, Y. (2004). Characterization of heavy metal particles embedded in tire dust. *Environment International*, *30*(8), 1009–1017. https://doi.org/10.1016/j.envint.2004.04.004

Battelle, (2012). Environmental technology verification report. Retrieved from http://cooperenvironmental.com/wp-content/uploads/2014/09/Xact625_ETVReport-full.pdf

Borai, E. H., El-Sofany, E. A., Abdel-Halim, A. S., & Soliman, A. A. (2002). Speciation of hexavalent chromium in atmospheric particulate samples by selective extraction and ion chromatographic determination. *Trac-Trend Analytical Chemistry*, *21*(11), 741–745. https://doi.org/10.1016/S0165-9936(02)01102-0

Brown, S. G., Eberly, S., Paatero, P., & Norris, G. A. (2015). Methods for estimating uncertainty in PMF solutions: Examples with ambient air and water quality data and guidance on reporting PMF results. *Science of the Total Environment*, *518-519*, 626–635. https://doi.org/10.1016/j.scitotenv.2015.01.022

Canagaratna, M. R., Jimenez, J. L., Kroll, J. H., Chen, Q., Kessler, S. H., Massoli, P., et al. (2015). Elemental ratio measurements of organic compounds using aerosol mass spectrometry: Characterization, improved calibration, and implications. *Atmospheric Chemistry and Physics*, *15*(1), 253–272. https://doi.org/10.5194/acp-15-253-2015

Canonaco, F., Slowik, J. G., Baltensperger, U., & Prevot, A. S. H. (2015). Seasonal differences in oxygenated organic aerosol composition: Implications for emissions sources and factor analysis. *Atmospheric Chemistry and Physics*, *15*(12), 6993–7002. https://doi.org/10.5194/acp-15-6993-2015

Chen, J., Liu, G. J., Kang, Y., Wu, B., Sun, R. Y., Zhou, C. C., & Wu, D. (2013). Atmospheric emissions of F, As, Se, Hg, and Sb from coal-fired power and heat generation in China. *Chemosphere*, *90*(6), 1925–1932. https://doi.org/10.1016/j.chemosphere.2012.10.032

Crippa, M., Canonaco, F., Slowik, J. G., El Haddad, I., DeCarlo, P. F., Mohr, C., et al. (2013). Primary and secondary organic aerosol origin by combined gas-particle phase source apportionment. *Atmospheric Chemistry and Physics*, *13*(16), 8411–8426. https://doi.org/10.5194/acp-13-8411-2013

Du, W. J., Zhang, Y. R., Chen, Y. T., Xu, L. L., Chen, J. S., Deng, J. J., et al. (2017). Chemical Characterization and Source Apportionment of PM2.5 during Spring and Winter in the Yangtze River Delta, China. *Aerosol and Air Quality Research*, *17*(9), 2165–2180. https://doi.org/10.4209/aaqr.2017.03.0108

Feng, J., Li, M., Zhang, P., Gong, S., Zhong, M., Wu, M., et al. (2013). Investigation of the sources and seasonal variations of secondary organic aerosols in PM2.5 in Shanghai with organic tracers. *Atmospheric Environment*, *79*, 614–622. https://doi.org/10.1016/j.atmosenv.2013.07.022

Feng, J. L., Sun, P., Hu, X. L., Zhao, W., Wu, M. H., & Fu, J. M. (2012). The chemical composition and sources of PM2.5 during the 2009 Chinese New Year's holiday in Shanghai. *Atmospheric Research*, *118*, 435–444. https://doi.org/10.1016/j.atmosres.2012.08.012

Gao, J., Peng, X., Chen, G., Xu, J., Shi, G. L., Zhang, Y. C., & Feng, Y. C. (2016). Insights into the chemical characterization and sources of PM2.5 in Beijing at a 1-h time resolution. *Science of the Total Environment*, *542*(Pt A), 162–171. https://doi.org/10.1016/j.scitotenv.2015.10.082

Griffith, S. M., Huang, X. H. H., Louie, P. K. K., & Yu, J. Z. (2015). Characterizing the thermodynamic and chemical composition factors controlling PM2.5 nitrate: Insights gained from two years of online measurements in Hong Kong. *Atmospheric Environment*, *122*, 864–875. https://doi.org/10.1016/j.atmosenv.2015.02.009

Ho, K. F., Lee, S. C., Chow, J. C., & Watson, J. G. (2003). Characterization of PM10 and PM2.5 source profiles for fugitive dust in Hong Kong. *Atmospheric Environment*, *37*(8), 1023–1032. https://doi.org/10.1016/S1352-2310(02)01028-2

Hu, D., Bian, Q. J., Lau, A. K. H., & Yu, J. Z. (2010). Source apportioning of primary and secondary organic carbon in summer PM2.5 in Hong Kong using positive matrix factorization of secondary and primary organic tracer data. *Journal of Geophysical Research*, *115*, D16204. https://doi.org/10.1029/2009JD012498

Huang, C., Chen, C. H., Li, L., Cheng, Z., Wang, H. L., Huang, H. Y., et al. (2011). Emission inventory of anthropogenic air pollutants and VOC species in the Yangtze River Delta region, China. *Atmospheric Chemistry and Physics*, *11*(9), 4105–4120. https://doi.org/10.5194/acp-11-4105-2011

Huang, R. J., Zhang, Y., Bozzetti, C., Ho, K. F., Cao, J. J., Han, Y., et al. (2014). High secondary aerosol contribution to particulate pollution during haze events in China. *Nature*, *514*(7521), 218–222. https://doi.org/10.1038/nature13774

Huggins, F. E., & Huffman, G. P. (1995). Chlorine in coal - an XAFS spectroscopic investigation. *Fuel*, *74*(4), 556–569. https://doi.org/10.1016/0016-2361(95)98359-M

Jeong, C. H., Wang, J. M., & Evans, G. J. (2016). Source apportionment of urban particulate matter using hourly resolved trace metals, organics, and inorganic aerosol components. *Atmospheric Chemistry and Physics Discussions*, 1–32. https://doi.org/10.5194/acp-2016-189

Karar, K., Gupta, A. K., Kumar, A., & Biswas, A. K. (2006). Characterization and identification of the sources of chromium, zinc, lead, cadmium, nickel, manganese and iron in PM10 particulates at the two sites of Kolkata, *India*. *Environmental Monitoring and Assessment*, *120*(1–3), 347–360. https://doi.org/10.1007/s10661-005-9067-7

Kim, Y. J., Kim, M. J., Lee, K. H., & Park, S. S. (2006). Investigation of carbon pollution episodes using semi-continuous instrument in Incheon, Korea. *Atmospheric Environment*, *40*(22), 4064–4075. https://doi.org/10.1016/j.atmosenv.2006.03.028

Li, H., Ma, Y. L., Duan, F. K., He, K. B., Zhu, L. D., Huang, T., et al. (2017). Typical winter haze pollution in Zibo, an industrial city in China: Characteristics, secondary formation, and regional contribution. *Environmental Pollution*, *229*, 339–349. https://doi.org/10.1016/j.envpol.2017.05.081

Li, L., An, J. Y., Zhou, M., Yan, R. S., Huang, C., Lu, Q., et al. (2015). Source apportionment of fine particles and its chemical components over the Yangtze River Delta, China during a heavy haze pollution episode. *Atmospheric Environment*, *123*, 415–429. https://doi.org/10.1016/j.atmosenv.2015.06.051

Li, L., Huang, C., Huang, H. Y., Wang, Y. J., Yan, R. S., Zhang, G. F., et al. (2014). An integrated process rate analysis of a regional fine particulate matter episode over Yangtze River Delta in 2010. *Atmospheric Environment*, *91*, 60–70. https://doi.org/10.1016/j.atmosenv.2014.03.053

Li, Y. Y., Chang, M. A., Ding, S. S., Wang, S. W., Ni, D., & Hu, H. T. (2017). Monitoring and source apportionment of trace elements in PM2.5: Implications for local air quality management. *Journal of Environmental Management*, *196*, 16–25. https://doi.org/10.1016/j.jenvman.2017.02.059

Li, Y. J., Sun, Y., Zhang, Q., Li, X., Li, M., Zhou, Z., & Chan, C. K. (2017). Real-time chemical characterization of atmospheric particulate matter in China: A review. *Atmospheric Environment*, *158*, 270–304. https://doi.org/10.1016/j.atmosenv.2017.02.027

Liu, B. S., Yang, J. M., Yuan, J., Wang, J., Dai, Q. L., Li, T. K., et al. (2017). Source apportionment of atmospheric pollutants based on the online data by using PMF and ME2 models at a megacity, China. *Atmospheric Research*, *185*, 22–31. https://doi.org/10.1016/j.atmosres.2016.10.023

Liu, S. Y., & Liang, X. Z. (2010). Observed diurnal cycle climatology of planetary boundary layer height. *Journal of Climate*, *23*(21), 5790–5809. https://doi.org/10.1175/2010JCLI3552.1

Makkonen, U., Virkkula, A., Mantykentta, J., Hakola, H., Keronen, P., Vakkari, V., & Aalto, P. P. (2012). Semi-continuous gas and inorganic aerosol measurements at a Finnish urban site: Comparisons with filters, nitrogen in aerosol and gas phases, and aerosol acidity. *Atmospheric Chemistry and Physics*, *12*(12), 5617–5631. https://doi.org/10.5194/acp-12-5617-2012

Malaguti, A., Mircea, M., La Torretta, T. M. G., Telloli, C., Petralia, E., Stracquadanio, M., & Berico, M. (2015). Comparison of online and offline methods for measuring fine secondary inorganic ions and carbonaceous aerosols in the Central Mediterranean area. *Aerosol and Air Quality Research*, *15*(7), 2641–2653. https://doi.org/10.4209/aaqr.2015.04.0240

Nel, A. (2005). Air pollution-related illness: Effects of particles. *Science*, *308*(5723), 804–806. https://doi.org/10.1126/science.1108752

Norris, G., Duvall, R., Brown, S., & Bai, S. (2014). EPA positive matrix factorization (PMF) 5.0 fundamentals and user guide prepared for the US Environmental Protection Agency Office of Research and Development, Washington, DC.

Paatero, P., Eberly, S., Brown, S. G., & Norris, G. A. (2014). Methods for estimating uncertainty in factor analytic solutions. *Atmospheric Measurement Techniques*, *7*(3), 781–797. https://doi.org/10.5194/amt-7-781-2014

Paatero, P., & Tapper, U. (1994). Positive matrix factorization—A nonnegative factor model with optimal utilization of error-estimates of data values. *Environmetrics*, *5*(2), 111–126. https://doi.org/10.1002/env.3170050203

Pant, P., & Harrison, R. M. (2013). Estimation of the contribution of road traffic emissions to particulate matter concentrations from field measurements: A review. *Atmospheric Environment*, *77*, 78–97. https://doi.org/10.1016/j.atmosenv.2013.04.028

Peng, X., Shi, G. L., Gao, J., Liu, J. Y., HuangFu, Y. Q., Ma, T., et al. (2016). Characteristics and sensitivity analysis of multiple-time-resolved source patterns of PM2.5 with real time data using Multilinear Engine 2. *Atmospheric Environment*, *139*, 113–121. https://doi.org/10.1016/j.atmosenv.2016.05.032

Phillips-Smith, C., Jeong, C. H., Healy, R. M., Zlotorzynska, E. D., Celo, V., Brook, J. R., & Evans, G. (2017). Sources of particulate matter in the Athabasca oil sands region: Investigation through a comparison of trace element measurement methodologies. *Atmospheric Chemistry and Physics*, *17*, 9435–9449. https://doi.org/10.5194/acp-17-9435-2017

Qiao, L. P., Cai, J., Wang, H. L., Wang, W. B., Zhou, M., Lou, S. R., et al. (2014). PM2.5 constituents and hospital emergency-room visits in Shanghai, China. *Environmental Science & Technology*, *48*(17), 10,406–10,414. https://doi.org/10.1021/es501305k

Qiao, T., Zhao, M., Xiu, G., & Yu, J. (2016). Simultaneous monitoring and compositions analysis of PM1 and PM2.5 in Shanghai: Implications for characterization of haze pollution and source apportionment. *Science of the Total Environment*, *557*, 386–394.

Ramanathan, V., Crutzen, P. J., Kiehl, J. T., & Rosenfeld, D. (2001). Atmosphere—Aerosols, climate, and the hydrological cycle. *Science*, *294*(5549), 2119–2124. https://doi.org/10.1126/science.1064034

Reff, A., Eberly, S. I., & Bhave, P. V. (2007). Receptor modeling of ambient particulate matter data using positive matrix factorization: Review of existing methods. *Journal of the Air & Waste Management Association*, *57*(2), 146–154. https://doi.org/10.1080/10473289.2007.10465319

Richard, A., Gianini, M. F. D., Mohr, C., Furger, M., Bukowiecki, N., Minguillón, M. C., et al. (2011). Source apportionment of size and time resolved trace elements and organic aerosols from an urban courtyard site in Switzerland. *Atmospheric Chemistry and Physics*, *11*(17), 8945–8963. https://doi.org/10.5194/acp-11-8945-2011

Seinfeld, J. H., & Pandis, S. N. (2006). *Atmospheric chemistry and physics: from air pollution to climate change* (p. 1203). New York: Wiley, John & Sons, Incorporated.

Sofowote, U. M., Rastogi, A. K., Debosz, J., & Hopke, P. K. (2014). Advanced receptor modeling of near-real-time, ambient PM2.5 and its associated components collected at an urban-industrial site in Toronto, Ontario. *Atmospheric Pollution Research*, *5*(1), 13–23. https://doi.org/10.5094/Apr.2014.003

Sun, Y. L., Wang, Z. F., Fu, P. Q., Yang, T., Jiang, Q., Dong, H. B., et al. (2013). Aerosol composition, sources and processes during wintertime in Beijing, China. *Atmospheric Chemistry and Physics*, *13*(9), 4577–4592. https://doi.org/10.5194/acp-13-4577-2013

Sun, Y. L., Zhuang, G. S., Tang, A. H., Wang, Y., & An, Z. S. (2006). Chemical characteristics of PM2.5 and PM10 in haze-fog episodes in Beijing. *Environmental Science & Technology*, *40*(10), 3148–3155. https://doi.org/10.1021/es051533g

ten Brink, H., Otjes, R., Jongejan, P., & Slanina, S. (2007). An instrument for semi-continuous monitoring of the size-distribution of nitrate, ammonium, sulphate and chloride in aerosol. *Atmospheric Environment*, *41*(13), 2768–2779. https://doi.org/10.1016/j.atmosenv.2006.11.041

Tian, Y. Z., Xiao, Z. M., Wang, H. T., Peng, X., Guan, L., Huangfu, Y. Q., et al. (2017). Influence of the sampling period and time resolution on the PM source apportionment: Study based on the high time-resolution data and long-term daily data. *Atmospheric Environment*, *165*, 301–309. https://doi.org/10.1016/j.atmosenv.2017.07.003

Vejahati, F., Xu, Z. H., & Gupta, R. (2010). Trace elements in coal: Associations with coal and minerals and their behavior during coal utilization —A review. *Fuel*, *89*(4), 904–911. https://doi.org/10.1016/j.fuel.2009.06.013

Vossler, T., Cernikovsky, L., Novak, J., & Williams, R. (2016). Source apportionment with uncertainty estimates of fine particulate matter in Ostrava, Czech Republic using positive matrix factorization. *Atmospheric Pollution Research*, *7*(3), 503–512. https://doi.org/10.1016/j.apr.2015.12.004

Wang, H. L., An, J. L., Cheng, M. T., Shen, L. J., Zhu, B., Li, Y., et al. (2016). One year online measurements of water-soluble ions at the industrially polluted town of Nanjing, China: Sources, seasonal and diurnal variations. *Chemosphere*, *148*, 526–536. https://doi.org/10.1016/j.chemosphere.2016.01.066

Wang, H. L., Qiao, L. P., Lou, S. R., Zhou, M., Chen, J. M., Wang, Q., et al. (2015). PM2.5 pollution episode and its contributors from 2011 to 2013 in urban Shanghai, China. *Atmospheric Environment*, *123*, 298–305. https://doi.org/10.1016/j.atmosenv.2015.08.018

Wang, Q. Q., He, X., Huang, X. H. H., Griffith, S. M., Feng, Y. M., Zhang, T., et al. (2017). Impact of secondary organic aerosol tracers on tracer-based source apportionment of organic carbon and $PM_{2.5}$: A case study in the Pearl River Delta, China. *ACS Earth and Space Chemistry*, *1*(9), 562–571. https://doi.org/10.1021/acsearthspacechem.7b00088

Wang, Y. J., Li, L., Chen, C., Huang, C., Huang, H., Feng, J., et al. (2014). Source apportionment of fine particulate matter during autumn haze episodes in Shanghai, China. *Journal of Geophysical Research: Atmospheres*, *119*, 1903–1914. https://doi.org/10.1002/2013JD019630

Williams, B. J., Goldstein, A. H., Kreisberg, N. M., & Hering, S. V. (2006). An in-situ instrument for speciated organic composition of atmospheric aerosols: Thermal Desorption Aerosol GC/MS-FID (TAG). *Aerosol Science and Technology*, *40*(8), 627–638. https://doi.org/10.1080/02786820600754631

Ye, B. M., Ji, X. L., Yang, H. Z., Yao, X. H., Chan, C. K., Cadle, S. H., et al. (2003). Concentration and chemical composition of PM2.5 in Shanghai for a 1-year period. *Atmospheric Environment*, *37*(4), 499–510. https://doi.org/10.1016/S1352-2310(02)00918-4

Zhao, M. F., Huang, Z. S., Qiao, T., Zhang, Y. K., Xiu, G. L., & Yu, J. Z. (2015). Chemical characterization, the transport pathways and potential sources of PM2.5 in Shanghai: Seasonal variations. *Atmospheric Research*, *158*, 66–78. https://doi.org/10.1016/j.atmosres.2015.02.003

Zhao, M. J., Zhang, Y., Ma, W. C., Fu, Q. Y., Yang, X., Li, C. L., et al. (2013). Characteristics and ship traffic source identification of air pollutants in China's largest port. *Atmospheric Environment*, *64*, 277–286. https://doi.org/10.1016/j.atmosenv.2012.10.007